Article

# Short- and Long-Range Order in the Positive Electrode Material, Li(NiMn)O: A Joint X-ray and Neutron Diffraction, Pair Distribution Function Analysis and NMR Study

Julien Brger, Nicolas Dupr, Peter J. Chupas, Peter L. Lee, Thomas Proffen, John B. Parise, and Clare P. Grey

*J. Am. Chem. Soc.*, **2005**, 127 (20), 7529-7537• DOI: 10.1021/ja050697u • Publication Date (Web): 26 April 2005



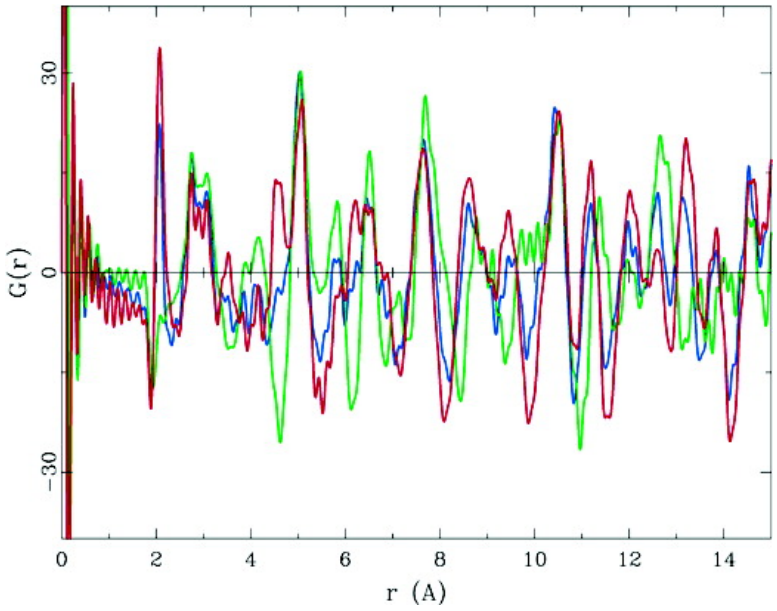


## More About This Article

Additional resources and features associated with this article are available within the HTML version:

- Supporting Information
- Links to the 9 articles that cite this article, as of the time of this article download
- Access to high resolution figures
- Links to articles and content related to this article
- Copyright permission to reproduce figures and/or text from this article

View the Full Text HTML

J|A|C|S
ARTICLES
Published on Web 04/26/2005

# Short- and Long-Range Order in the Positive Electrode Material, $Li(NiMn)_{0.5}O_2$: A Joint X-ray and Neutron Diffraction, Pair Distribution Function Analysis and NMR Study

Julien Bréger,[†] Nicolas Dupré,[†] Peter J. Chupas,[‡] Peter L. Lee,[‡] Thomas Proffen,[§] John B. Parise,[†] and Clare P. Grey*[,†]

*Contribution from the Department of Chemistry, State University of New York at Stony Brook, Stony Brook, New York 11794, Materials Science Division and Advanced Photon Source, Argonne National Laboratory, Argonne, Illinois 60439, and Los Alamos Neutron Science Center, Los Alamos National Laboratory, Los Alamos, New Mexico 87545*

Received February 2, 2005; E-mail: cgrey@notes.cc.sunysb.edu

***Abstract:*** The local environments and short-range ordering of $LiNi_{0.5}Mn_{0.5}O_2$, a potential Li-ion battery positive electrode material, were investigated by using a combination of X-ray and neutron diffraction and isotopic substitution (NDIS) techniques, $^6$Li Magic Angle Spinning (MAS) NMR spectroscopy, and for the first time, X-ray and neutron Pair Distribution Function (PDF) analysis, associated with Reverse Monte Carlo (RMC) calculations. Three samples were studied: $^6Li(NiMn)_{0.5}O_2$, $^7Li(NiMn)_{0.5}O_2$, and $^7Li(NiMn)_{0.5}O_2$ enriched with $^{62}$Ni (denoted as $^7Li^{ZERO}Ni_{0.5}Mn_{0.5}O_2$), so that the resulting scattering length of Ni atoms is null. $LiNi_{0.5}Mn_{0.5}O_2$ adopts the $LiCoO_2$ structure (space group $R\bar{3}m$) and comprises separate lithium layers, transition metal layers (Ni, Mn), and oxygen layers. NMR experiments and Rietveld refinements show that there is approximately 10% of Ni/Li site exchange between the Li and transition metal layers. PDF analysis of the neutron data revealed considerable local distortions in the layers that were not captured in the Rietveld refinements performed using the Bragg diffraction data and the $LiCoO_2$ structure, resulting in different M−O bond lengths of 1.93 and 2.07 Å for Mn−O and Ni/Li−O, respectively. Large clusters of 2400−3456 atoms were built to investigate cation ordering. The RMC method was then used to improve the fit between the calculated model and experimental PDF data. Both NMR and RMC results were consistent with a nonrandom distribution of Ni, Mn, and Li cations in the transition metal layers; both the Ni and Li atoms are, on average, close to more Mn ions than predicted based on a random distribution of these ions in the transition metal layers. Constraints from both experimental methods showed the presence of short-range order in the transition metal layers comprising $LiMn_6$ and $LiMn_5Ni$ clusters combined with Ni and Mn contacts resembling those found in the so-called "flower structure" or structures derived from ordered honeycomb arrays.

## Introduction

Layered lithium nickel manganese oxides are promising, cheap, and nontoxic alternative positive electrode materials to the commercial $LiCoO_2$ electrode used in Li-ion batteries. Among these materials, $LiNi_{0.5}Mn_{0.5}O_2$ is one of the most attractive, due to its high theoretical capacity (280 mAh/g). In 2001, Ohzuku et al.[1,2] obtained a stable capacity of 200 mAh/g between 2.5 and 4.5 V up to 30 cycles, while Lu et al.[3] reported that a material with the same nominal composition gives a capacity of 160 mAh/g when the cycling process is performed between 2.0 and 4.6 V. The $Ni^{2+}$ ions are electrochemically active in this material, the Mn ions remaining as $Mn^{4+}$ throughout the cycling process.[4−6] This compound represents the end member of continuous solid solution between $LiNi_{0.5}Mn_{0.5}O_2$ and $Li_2MnO_3$, in which compounds with low Ni content, such as $Li(Ni_{1/3}Mn_{5/9}Li_{1/9})O_2$, exhibit strong $Li_2MnO_3$-like ordering.

$LiNi_{0.5}Mn_{0.5}O_2$ is a layered material that adopts the α-$NaFeO_2$ structure (space group $R\bar{3}m$, No. 166, Figure 1).[7] $Li_2MnO_3$ may also be viewed as a layered material, and its formula may be rewritten as $Li[Li_{1/3}Mn_{2/3}]O_2$, in the notation used for these layered compounds. The Li and Mn atoms in the Li/Mn layers of $Li_2MnO_3$ are ordered, forming a "honeycomb" arrangement (Figure 2a). Li MAS NMR experiments also found $Li^+$ ions in the transition metal (TM) layers of $LiNi_{0.5}Mn_{0.5}O_2$, presumably caused by a $Ni^{2+}$ substitution in the lithium layers due to the similar size of $Li^+$ and $Ni^{2+}$ cations. $Li^+/Mn^{4+}$, $Li_2MnO_3$-like, ordering was suggested to provide a driving force for the $Li^+/$

[†] State University of New York at Stony Brook.
[‡] Argonne National Laboratory.
[§] Los Alamos National Laboratory.

(1) Ohzuku, T.; Makimura, Y. *Chem. Lett.* **2001**, 744.
(2) Makimura, Y.; Ohzuku, T. *J. Power Sources* **2003**, *119*−*121*, 156.
(3) Lu, Z.; MacNeil, D. D.; Dahn, J. R. *Electrochem. Solid State Lett.* **2001**, *4*, A191.
(4) Yoon, W.-S.; Grey, C. P.; Balasubramanian, M.; Yang, X.-Q.; McBreen, J. *Chem. Mater.* **2003**, *15*, 3161.
(5) Kobayashi, H.; Sakaebe, H.; Kageyma, H.; Tatsumi, K.; Arachi, Y.; Kamiyama, T. *J. Mater. Chem.* **2003**, *13*, 590.
(6) Johnson, C. S.; Kim, J. S.; Kropf, A. J.; Kahaian, A. J.; Vaughey, J. T.; Fransson, L. M. L.; Edström, K.; Thackeray, M. M. *Chem. Mater.* **2003**, *15*, 2313.
(7) Mizushima, K.; Jones, P. C.; Wiseman, P. J.; Goodenough, J. B. *Mater. Res. Bull.* **1980**, *15*, 783.

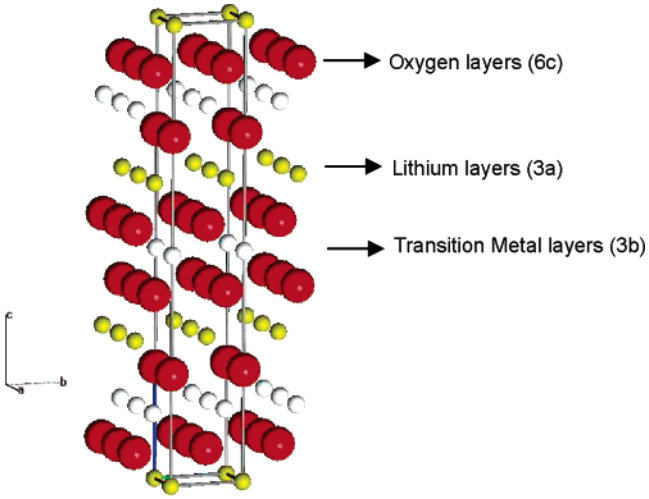


***Figure 1.*** Ideal structural model of $LiNi_{0.5}Mn_{0.5}O_2$ based on $LiCoO_2$ ($\alpha$-$NaFeO_2$ structure, space group $R\bar{3}m$, $a = b = 2.8874$ Å, $c = 14.2825$ Å, and $\gamma = 120°$).[7] Each atom in every layer is surrounded by six atoms in the same layer. Li atoms are on the 3a sites; Ni and Mn atoms share the 3b sites, and O atoms are on the 6c sites (with $z = 0.2424$).

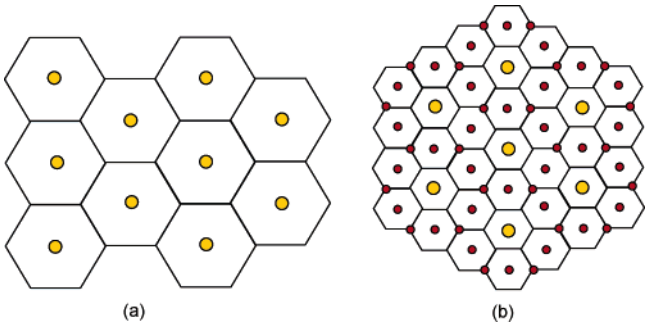


***Figure 2.*** (a) A view of the honeycomb ordering found in the *ab* planes of $Li_2MnO_3$ along the *c*-axis. Each Li atom (in yellow) in the Li/Mn layers is surrounded by six Mn atoms at the corners of the hexagons. (b) The transition metal layers in the proposed[10] flower structure of $Li(NiMn)_{0.5}O_2$. The Li, Ni, and Mn atoms are in yellow, red, and at the empty corners of the hexagons, respectively.

$Ni^{2+}$ exchange.[8,9] These results are consistent with the X-ray and neutron diffraction study by Lu et al.,[11,12] where acceptable structure refinements were obtained by allowing a partial exchange between the Ni and Li ions. More recently, Makimura et al.[2] also found that approximately 8−10% of the Ni ions are displaced from the TM to the Li layers.

Previous Li MAS NMR experiments on $LiNi_{0.5}Mn_{0.5}O_2$ showed a much stronger tendency for the $Li^+$ in the TM layers to be surrounded by 5 or 6 $Mn^{4+}$ ions, over that calculated for a random arrangement of the $Li^+$, $Ni^{2+}$, and $Mn^{4+}$ ions in these layers.[8,9] EXAFS studies on both the Ni and Mn K-edges were consistent with preferential ordering of Li near Mn, and local cation environments for Ni and Mn of $Mn(M_{5.2}Li_{0.8})$ and Ni-($M_6$) (M = Ni, Mn) were obtained, where only the cations in the local coordination shell in the TM layers are considered.[4] Unfortunately, EXAFS experiments cannot determine whether the Ni or Mn ions preferentially order near Ni/Mn in the first coordination shell, due to the similar electron densities of these ions. More recently, first principle calculations by Van der Ven and Ceder showed that the so-called "flower structure" (Figure 2b), where the Li in TM layers are surrounded by six Mn atoms in the first coordination sphere and by Ni atoms in the second coordination sphere, represents the lowest energy arrangement of the cations.[10]

The structural properties of insertion electrode materials and the ordering of the different cations are strongly related to their electrochemical performance. For example, previous ex situ NMR experiments on charged samples have shown that the Li ions located in the TM layers participate in the electrochemistry and cannot be considered as an inert part of the structure.[8] Furthermore, ab initio calculations for this system have shown a strong correlation between cation ordering and the insertion voltages for Li removal from both the Li layers and the TM layers.[9,10,13] Although NMR results have provided information concerning the short-range order surrounding Li, additional probes of structure are required to investigate order surrounding the TM ions. Thus, high-energy X-ray and neutron diffraction techniques, coupled with Pair Distribution Function (PDF) analysis and $^6$Li NMR, were used to study the local and long-range structure of $LiNi_{0.5}Mn_{0.5}O_2$. Although PDF analysis has been used to study nanocrystalline alkali metal manganese oxides, Reverse Monte Carlo (RMC) techniques have not been applied to this class of materials[14] to improve the fit between the experimental and calculated PDF and to investigate the nature of cation ordering and the local structure. By combining two methods that are sensitive to local cation environments, and long-range order, clear constraints can be obtained, which can be used to generate a detailed model of the structure of this material.

## Materials and Methods

**Pair Distribution Function Analysis.** Pair Distribution Function (PDF) analysis was used to study the chemical short-range order, which is not always readily available from X-ray or neutron diffraction patterns.[15] Indeed, traditional X-ray or neutron diffraction analysis considers only the Bragg scattering, which contains information about the long-range average structure, whereas the PDF technique uses the total scattering (Bragg and diffuse scatterings). Like NMR, PDF analysis can provide information about the local structure and, thus, the presence of ordering. The method is briefly discussed in this section before outlining the experimental details associated with sample preparation and characterization.

The PDF $G(r)$ gives the probability of finding an atom at a given distance $r$ from another atom and can be considered as a bond length distribution. It is obtained from the powder diffraction (X-ray or neutron) via a Fourier transform of the normalized scattering intensity, $S(Q)$:[16]

$$G(r) = 4\pi r[\rho(r) - \rho_0] = \frac{2}{\pi}\int_0^\infty Q[S(Q) - 1]\sin(Qr)dQ$$

where $\rho(r)$ is the microscopic pair density, $\rho_0$ is the average number

(8) Yoon, W.-S.; Paik, Y.; Yang, X.-Q.; Balasubramanian, M.; McBreen, J.; Grey, C. P. *Electrochem. Solid State Lett.* **2002**, *5*, A263.
(9) Yoon, W.-S.; Iannopollo, S.; Grey, C. P.; Carlier, D.; Gorman, J.; Reed, J.; Ceder, G. *Electrochem. Solid State Lett.* **2004**, *7*, A167.
(10) Van der Ven, A.; Ceder, G. *Electrochem. Commun.* **2004**, *6*, 1045.
(11) Lu, Z.; Dahn, J. R. *J. Electrochem. Soc.* **2002**, *149*, A815.
(12) Lu, Z.; Beaulieu, L. Y.; Donaberger, R. A.; Thomas, C. L.; Dahn, J. R. *J. Electrochem. Soc.* **2002**, *149*, A778.
(13) Reed, J.; Ceder, G. *Electrochem. Solid State Lett.* **2002**, *5*, A145.
(14) Gateshki, M.; Hwang, S.-J.; Park, D. H.; Ren, Y.; Petkov, V. *J. Phys. Chem. B* **2004**, *108*, 14956.
(15) Proffen, Th.; Billinge, S. J. L.; Egami, T.; Louca, D. *Z. Kristallogr.* **2003**, *218*, 132.
(16) Egami, T.; Billinge, S. J. L. In *Underneath the Bragg Peaks: Structure Analysis of Complex Materials*; Cahn, R., Ed.; Oxford/Pergamon Press: New York, 2004.

***Table 1.*** Coherent Neutron Scattering Lengths $b_i$ (fm) of the Different Isotopes

| $^6$Li | $^7$Li | $^{nat}$Li | $^{62}$Ni | $^{nat}$Ni | Mn | O |
|---|---|---|---|---|---|---|
| 2.00 | −2.22 | −1.90 | −8.7 | 10.3 | −3.73 | 5.80 |

density, and $Q$ is the magnitude of the scattering vector ($Q = (4\pi\sin\theta)/\lambda$). One problem with the Fourier transform is that it is not possible to measure data up to infinite $Q$. The cutoff at finite $Q_{max}$ decreases the real space resolution of the PDF and causes some termination ripples. For both X-ray and neutron scattering experiments, high energies are required in order to access high values of $Q_{max}$; data suitable for PDF analysis can be obtained at high-energy synchrotron X-ray and spallation neutron sources, respectively.

After obtaining an experimental PDF, the first information provided by the data is the bond lengths. It is also possible to calculate the PDF $G_c(r)$ in order to refine a structural model, using the relation[16]

$$G_c(r) = \frac{1}{r}\sum_i\sum_j\left[\frac{b_i b_j}{\langle b\rangle^2}\delta(r - r_{ij})\right] - 4\pi r\rho_0$$

The sum is performed over all pairs of atoms $i$ and $j$ separated by $r_{ij}$. The scattering power of the atom $i$ is given by the value of $b_i$, and $<b>$ is the average scattering power of the sample. The value of $b_i$ is, in the case of neutrons and X-rays, given by the scattering length and the atomic factor at a given $Q$, respectively. For neutrons, the intensity of a peak can be negative if one of the two atoms has a negative coherent scattering length $b_i$. By changing the scattering length of one or more elements, it is possible to extract a chemically specific PDF. In the case of neutrons, one can use isotopic substitution since different isotopes of an element have different neutron scattering lengths. In addition, an appropriate mixing of two different isotopes of the same element, which have coherent neutron scattering lengths with opposite signs (such as $^{nat}$Ni and $^{62}$Ni in this experiment), results in a null scattering from this element.

**Sample Preparation.** $Li(NiMn)_{0.5}O_2$ powders were prepared by the double mixed hydroxide method.[3] A 50 mL aqueous solution of stoichiometric amounts of transition metal nitrates was prepared and slowly dripped (1−2 h) into 400 mL of a stirred solution of LiOH using a buret, yielding a precipitation of $M(OH)_2$, where M = Mn and Ni, with a homogeneous cation distribution. The dried precipitate was mixed with $Li(OH)\cdot H_2O$ in stoichiometric proportions. The mixture was then heated in air at 480 °C for 12 h, annealed at 900 °C for another 12 h, and quenched using liquid nitrogen.

To determine the local environment of each atom independently, neutron diffraction experiments were performed on $Li(NiMn)_{0.5}O_2$ powders with different isotopes. Three sets of samples were prepared: $^6Li(NiMn)_{0.5}O_2$, $^7Li(NiMn)_{0.5}O_2$, and $^7Li(NiMn)_{0.5}O_2$ enriched with $^{62}$Ni (denoted as $^7Li^{ZERO}Ni_{0.5}Mn_{0.5}O_2$), so that the resulting scattering length of the Ni atoms is null (the coherent scattering lengths are listed in Table 1;[17] a molar $^{62}Ni/^{nat}Ni$ ratio of 1.184 was used, with $^{nat}$Ni denoting natural abundant Ni). The first two samples were prepared with either $^6Li(OH)\cdot H_2O$ (Cambridge Isotopes, 90−95%) or $^7Li(OH)\cdot H_2O$ (Aldrich, >97%). In the case of the $^7Li(^{ZERO}NiMn)_{0.5}O_2$, the nickel nitrate was first prepared by dissolving a mixture of $^{nat}$Ni (Aldrich, 99.99%) and $^{62}$Ni metal (Isotec, >99%), with a weight ratio $^{62}Ni/^{nat}Ni$ of 1.250, in a nitric acid aqueous solution, so that the final solution contains only the nickel nitrate and no excess of nitric acid. This was checked by measuring the pH during the mixed hydroxide precipitation to ensure a basic solution with a pH of 12.

**Electrochemistry.** The cathodes were prepared by mixing 80 wt % of active material, 10 wt % of acetylene black as an electronic conductor, and 10 wt % of polyvinylidene fluoride binder (PVDF) in cyclopentanone. The slurry was deposited on an aluminum plate and dried at 80 °C until the solvent had evaporated completely. Swagelok-type cells were assembled in an argon-filled glovebox. Each cell contains typically about 20 mg of active material, separated from a lithium foil by glass microfiber filters. A 1 M solution of $LiPF_6$ in ethylene carbonate:dimethyl carbonate (1:1) has been used as the electrolyte. Electrochemical experiments were carried out on a battery cycler (Arbin Instruments, College Station, Texas) in galvanostatic mode at a C/20 rate, between 2.0 and 4.6 V.

**X-ray Diffraction.** X-ray diffraction (XRD) was used to confirm the presence of the desired structure of the starting materials and the purity of the samples. XRD was performed by using a Scintag powder X-ray diffractometer equipped with a Cu target X-ray tube (Cu K$\alpha$1:$\lambda$ = 1.5406 Å). A range of $2\theta$ values from 10 to 70° with a scanning rate of 1° per min and a step size of 0.02° was used.

To carry out the Pair Distribution Function (PDF) studies, X-ray synchrotron powder diffraction data of $^7Li(NiMn)_{0.5}O_2$ were collected at the 1-ID-XOR beamline at the Advanced Photon Source (APS), Argonne National Laboratory, IL. The PDF data were acquired using a two-dimensional image-plate (IP) detector, as previously described.[18] High-energy X-rays were delivered to the experimental hutch with a doubly bent Laue monochromator capable of providing a flux of $10^{12}$ photons/s. X-rays of 0.15359 Å wavelength at the gold absorption edge were utilized in this experiment. A $LaB_6$ standard was employed to calibrate the sample-to-detector distance and the tilt of the IP to the beam path. Data were obtained from the powder sample in transmission geometry. The IP data were integrated and converted to intensity readings versus $2\theta$ with the Fit2D software.[19] The PDF data were generated using PDFgetX.[20] The measured intensity was corrected from the absorption by the glass capillary by background subtraction. Corrections for multiple scattering, X-ray polarization, sample absorption, Compton scattering, and Laue diffuse scattering were then applied, as described in Chupas et al.,[18] to obtain the structure function $S(Q)$. A detector efficiency correction was also included.[21] Direct Fourier transform of the reduced structure function $F(Q) = Q[S(Q) - 1]$ up to $Q_{max} = 23$ Å$^{-1}$ gave $G(r)$, the pair distribution function.

**Neutron Diffraction.** Neutron diffraction experiments were performed on the General Materials Diffractometer (GEM) instrument at ISIS (Didcot, UK) for the pristine materials. The samples (from 300 mg to 1 g) were packed into 5 mm inside diameter thin-walled vanadium cans. The exposure time for each sample was approximately 12 h. The data were corrected for instrument background, sample and background absorption, and multiple scattering. Data up to $Q_{max} = 40$ Å$^{-1}$ were used in the Fourier transform. The PDF data obtained from these neutron experiments were processed by using the GUDRUN software.[22]

**MAS NMR Spectroscopy.** The $^6$Li MAS NMR experiment was performed with a double-resonance 2 mm probe, built by A. Samoson and co-workers, on a CMX-200 spectrometer using a magnetic field of 4.7 T. The spectrum was collected at an operating frequency of 29.46 MHz. A spinning frequency of 39 kHz and rotor-synchronized spin−echo sequence (90°-$\tau$-180°-$\tau$-acq) was used to acquire the spectra; $\pi/2$ pulses of 2.8 $\mu$s were used, with delay times of 0.2 s. The spectrum was referenced to 1 M $^6$LiCl solution at 0 ppm. To improve the resolution of the different resonances, a $^6$Li MAS NMR experiment with a spinning frequency of 70 kHz was performed with a double-resonance 1.5 mm probe, on a Bruker CXP-200 spectrometer again by using a magnetic field of 4.7 T.

(17) Sears, V. F. *Neutron News 3* **1992**, *3*, 26.

(18) Chupas, P. J.; Qiu, X.; Hanson, J. C.; Lee, P. L.; Grey, C. P.; Billinge, S. J. L. *J. Appl. Crystallogr.* **2003**, *36*, 1342.

(19) Hammersley, A. P. ESRF Internal Report, ESRF98HA01T, Fit2D V9.129 Reference Manual V3.1, 1998.

(20) Jeong, I.-K.; Thompson, J.; Proffen, Th.; Perez, A.; Billinge, S. J. L. *J. Appl. Crystallogr.* **2001**, *34*, 536.

(21) Coppens, P.; Leiserowitz, L.; Rabinovich, D. *Acta Crystallogr.* **1965**, *18*, 1035.

(22) Soper, A. K.; Buchanan, P. *Gudrun*, version 1.2, ISIS Report OX11OQX, 2001.

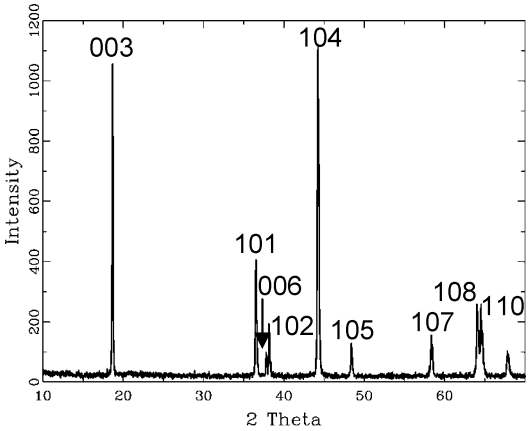


***Figure 3.*** XRD pattern of $^{7}LiNi_{0.5}Mn_{0.5}O_2$ synthesized at 900 °C for 12 h.

## Results and Analysis of the Diffraction Data

**Laboratory Diffraction.** The XRD pattern of $LiNi_{0.5}Mn_{0.5}O_2$ is displayed in Figure 3 and is similar to the pattern obtained for a single phase material with the ideal layered $LiCoO_2$ structure (Figure 1). All of the reflections can be indexed with the hexagonal setting of the rhombohedral $R\bar{3}m$ space group (No. 166), with Li on the 3a sites, transition metals on the 3b sites, and oxygen on the 6c sites.[7] As shown by Gummow and co-workers,[23] a large value for the ratio of the intensities of the 003:104 reflections and good resolution of the 006/012 and the 108/110 reflection pairs are typical of an ideal layered structure. The pairs of reflections are well resolved in our sample of $LiNi_{0.5}Mn_{0.5}O_2$, but in all of our XRD diffractograms, the 003 intensity is smaller than the 104 intensity. This is ascribed to the deviation from this ideal structure due to the presence of TM atoms in the lithium layers.[1,2] It may also arise from preferred orientation due to the use of the flat-plate geometry.

**Neutron Diffraction.** Figure 4 shows the neutron patterns of $^{7}Li(NiMn)_{0.5}O_2$, $^{7}Li(^{ZERO}NiMn)_{0.5}O_2$, and $^{6}Li(NiMn)_{0.5}O_2$. Rietveld[24] refinements of the structures were performed with GSAS-EXPGUI,[25] with these neutron diffraction data. In previous structure refinements,[11,12] only Ni atoms, and not Mn atoms, were clearly shown to move to the lithium layer, due to the similar size of $Ni^{2+}$ and $Li^{+}$ ions. Therefore, Ni/Li site exchange was allowed between the lithium and TM layers subject to a constraint that fixed the Ni/Li stoichiometry to the nominal Ni and Li concentrations. Good agreements are seen between the experimental data and patterns calculated with the $LiCoO_2$ structural model (space group $R\bar{3}m$). Close examination of the diffraction patterns revealed weaker peaks, which could not be indexed with the $R\bar{3}m$ space group. These peaks can, however, be indexed based on the larger $\sqrt{3}a \times \sqrt{3}a$ cell shown in Figure 2 and have been ascribed to $Li_2MnO_3$-like (honeycomb) ordered regions in the material.[26,27] The corresponding structural parameters obtained with the $R\bar{3}m$ model are listed in Table 2. The average refined percentage of Ni in Li layers is

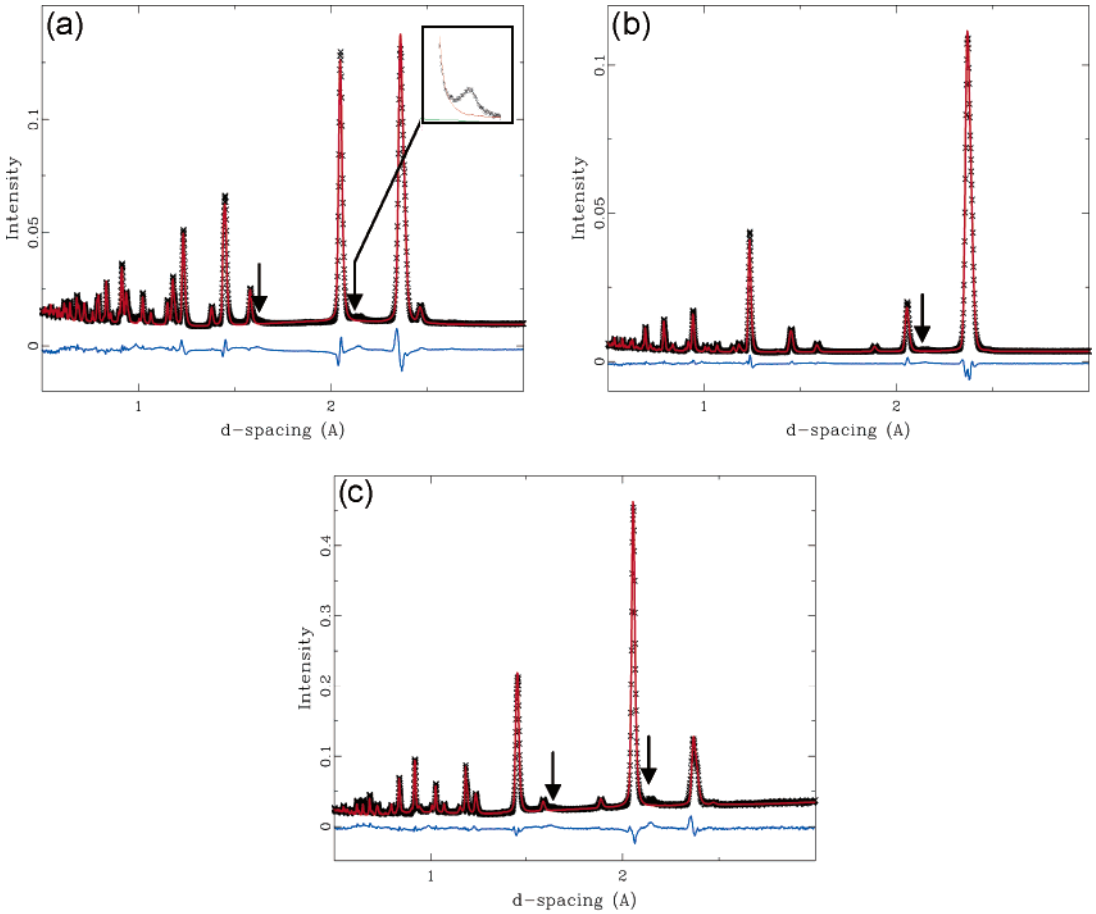


***Figure 4.*** Rietveld refinements using the neutron diffraction patterns (bank 4 from 50 to 75° of the GEM detector) of (a) $^{7}LiNi_{0.5}Mn_{0.5}O_2$, (b) $^{7}Li^{ZERO}Ni_{0.5}Mn_{0.5}O_2$, and (c) $^{6}LiNi_{0.5}Mn_{0.5}O_2$. The crosses and the solid red line represent the experimental data and the calculated pattern, respectively. The difference between the calculated and experimental patterns is shown in blue below the data. The arrows show the reflections coming from $Li_2MnO_3$-like ordering regions. The structural parameters are given in Table 2.

***Table 2.*** Rietveld Refinement Results for the Neutron Patterns

| | $^7LiNi_{0.5}Mn_{0.5}O_2$ | $^7Li^{ZERO}Ni_{0.5}Mn_{0.5}O_2$ | $^6LiNi_{0.5}Mn_{0.5}O_2$ |
|---|---|---|---|
| *a* (Å) | 2.8823(2) | 2.8914(2) | 2.89239(9) |
| *c* (Å) | 14.262(1) | 14.3006(9) | 14.2970(6) |
| *V* (Å$^3$) | 102.60(2) | 103.54(2) | 103.583(7) |
| *z*(O) | 0.24177(3) | 0.24235(2) | 0.24214(5) |
| 100*Uiso (Å$^2$) | | | |
| 3a sites (Li) | 4.1(2) | 2.58(6) | 0.56(6) |
| 3b sites (Ni, Mn) | 0.15(3) | 0.53(4) | 1.80(8) |
| 6c sites (O) | 1.04(1) | 1.17(1) | 2.05(3) |
| *n* Ni (3a)[a] (%) | 10.6(1) | 5.0(4) | 7.2(5) |
| bank 3 (25−45°) | Rwp = 4.66% | Rwp = 3.47% | Rwp = 5.23% |
| bank 4 (50−75°) | Rwp = 6.32% | Rwp = 4.63% | Rwp = 8.40% |
| bank 5 (79−104°) | Rwp = 6.01% | Rwp = 5.64% | Rwp = 8.73% |

[a] *n* Ni (3a) is the occupation of the 3a site (Li layers) by nickel. For each sample, we simultaneously refined three different histograms, corresponding to banks 3, 4, and 5 of the GEM detector, with the same parameters.

around 7.8 ± 2.8%. Differences in the Ni percentage are ascribed to the different Li and Ni scattering factors for Li/Ni in these samples. The diffraction pattern of $^7Li(^{ZERO}NiMn)_{0.5}O_2$ is much less sensitive to Li/Ni exchange than $^7Li(NiMn)_{0.5}O_2$, a change in the Li occupancy of the TM layers from 5 to 10% in $^7Li(^{ZERO}NiMn)_{0.5}O_2$ resulting in only a small change in $R_{wp}$ from 5.64 to 5.65% for bank 5 and no change for banks 3 and 4. Due to the strong absorption problems associated with $^6Li$ nuclei, $^6Li(NiMn)_{0.5}O_2$ is also less sensitive to Li/Ni exchange than $^7Li(NiMn)_{0.5}O_2$. Now, a change in the Li occupancy of the TM layers from 5 to 10% results in only a small change of $R_{wp}$ from 5.23 to 5.28% for bank 3 and no change for banks 4 and 5 for $^6Li(NiMn)_{0.5}O_2$. In contrast, this change results in a much larger change in $R_{wp}$ (from 7.65 to 4.66% for bank 3, and for a change from 5 to 10%) for $^7Li(NiMn)_{0.5}O_2$. Thus, the data obtained for $^7Li(NiMn)_{0.5}O_2$ are the most sensitive to the Li/Ni exchange, and the value of 10.6(1)% exchange of Li for Ni, used for the RMC calculations described later and consistent with NMR results, is considered to be the most precise.

**PDF.** The model used to describe the diffraction data is not able to model all of the weaker peaks ascribed to ordering of cations in the TM layers. To probe the source of this ordering further, the neutron Pair Distribution Function (PDF) was calculated for the three different samples: $^6Li(NiMn)_{0.5}O_2$, $^7Li(NiMn)_{0.5}O_2$, and $^7Li(^{ZERO}NiMn)_{0.5}O_2$ (Figure 5). This calculation uses all of the scattering data and is not dependent on the model used to describe the diffraction data. The intensities were normalized (to allow comparison between samples) by using the scale factors obtained from the Rietveld refinements for each sample. The first intense peak (at 1.93 Å) in the plot (of $G(r)$) corresponds to the shortest bond length. As shown before in the EXAFS experiments carried out by Yoon et al.[4] and Johnson et al.,[6] this corresponds to the $Mn^{4+}$−O distance. The intensity of this peak is negative, as the coherent scattering length of Mn atoms (see Table 1) is negative ($b$(Mn) = −3.73 fm) and barely changes between samples. The second peak is ascribed to the Ni/Li−O bonds since the change in the intensity of this peak follows the change in the coherent scattering length

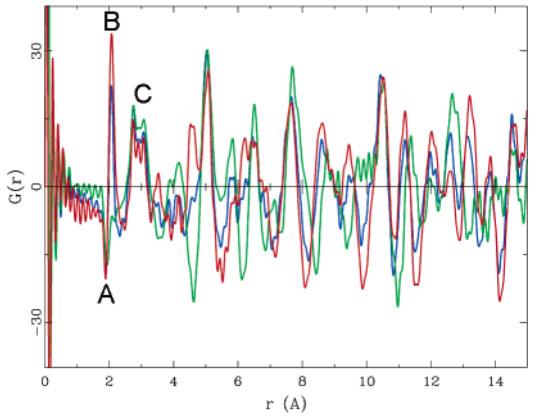


***Figure 5.*** Pair distribution functions (PDF, $G(r)$) of $^7LiNi_{0.5}Mn_{0.5}O_2$ (blue), $^7Li^{ZERO}Ni_{0.5}Mn_{0.5}O_2$ (green), and $^6LiNi_{0.5}Mn_{0.5}O_2$ (red) pristine materials. The PDF intensities were normalized by using the scale factors determined from the Rietveld refinements. The peaks assignments are: (A) Mn−O distances, (B) Ni−O and Li−O distances, and (C) M−M (where M = Ni, Mn, and Li) and O−O closest contacts.

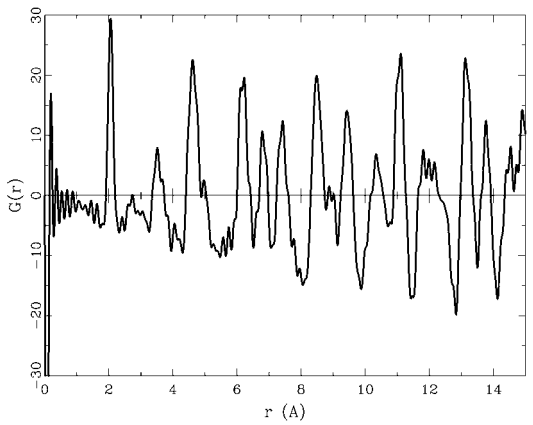


***Figure 6.*** Differential Ni PDF obtained from the PDF data of $^7Li(^{nat}NiMn)_{0.5}O_2$ and $^7Li(^{ZERO}NiMn)_{0.5}O_2$.

value between samples. The intensity of this peak is the greatest for $^6Li(NiMn)_{0.5}O_2$ ($b(^6Li)$ = 2.00 fm, $b$(Ni) = 10.3 fm), decreasing for $^7Li(NiMn)_{0.5}O_2$ ($b(^7Li)$ = −2.22 fm, $b$(Ni) = 10.3 fm), and becoming negative for $^7Li(^{ZERO}NiMn)_{0.5}O_2$ ($b(^7Li)$ = −2.22 fm, $b$(Ni) = 0.0 fm). However, the $Li^+$−O and $Ni^{2+}$−O distances are so close that the two peaks could not be resolved in this PDF data. The pairwise correlations involving at least one Ni atom (the differential Ni PDF; i.e., the Ni−O and Ni−M contacts) can be obtained by subtracting the $^7Li(^{ZERO}NiMn)_{0.5}O_2$ data from the $^7Li(NiMn)_{0.5}O_2$ data (Figure

(23) Gummow, R. J.; Thackeray, M. M.; David, W. I. F.; Hull, S. *Mater. Res. Bull.* **1992**, *27*, 327.
(24) Rietveld, H. M. *J. Appl. Crystallogr.* **1969**, *2*, 65.
(25) Larson, A. C.; Von Dreele, R. B. *General Structure Analysis System* (GSAS), Los Alamos National Laboratory Report LAUR 86-748, 2000; Toby, B. H. *J. Appl. Crystallogr.* **2001**, *34*, 210.
(26) Lu, Z.; Chen, Z.; Dahn, J. R. *Chem. Mater.* **2003**, *15*, 3214.
(27) Meng, Y. S.; Ceder, G.; Grey, C. P.; Yoon, W.-S.; Shao-Horn, Y. *Electrochem. Solid State Lett.* **2004**, *7*, A155.

***Table 3.*** Number of Li/Ni/Mn Pairs in the Transition Metal Layers (*ab* Plane) and Occupational Correlation Results before and after the RMC Calculations for Two Different Cluster Size

| | 10 × 10 × 2 Cluster | | 12 × 12 × 2 Cluster | |
|---|---|---|---|---|
| | before RMC | after RMC | before RMC | after RMC |
| %Ni−Ni pairs | 16.4 (295 pairs) | 12.0 (215 pairs) | 16.1 (418 pairs) | 11.8 (306 pairs) |
| %Ni−Mn pairs | 42.0 (755 pairs) | 50.5 (909 pairs) | 42.4 (1099 pairs) | 50.2 (1301 pairs) |
| %Mn−Mn pairs | 23.2 (418 pairs) | 19.1 (344 pairs) | 24.2 (626 pairs) | 20.7 (536 pairs) |
| %Li−Mn pairs | 8.9 (161 pairs) | 8.5 (155 pairs) | 9.1 (235 pairs) | 8.8 (227 pairs) |
| %Li−Ni pairs | 8.6 (155 pairs) | 8.9 (161 pairs) | 7.8 (201 pairs) | 8.1 (209 pairs) |
| %Li−Li pairs | 0.89 (16 pairs) | 0.89 (16 pairs) | 0.50 (13 pairs) | 0.5 (13 pairs) |
| total (%) | 100 (1800 pairs) | 100 (1800 pairs) | 100 (2592 pairs) | 100 (2592 pairs) |
| correlation $c_{NiMn}$[a] | −0.04 | −0.25 (±0.04) | −0.04 | −0.23 (±0.04) |
| correlation $c_{LiNi}$[a] | −0.04 | −0.11 (±0.1) | −0.09 | −0.16 (±0.1) |
| correlation $c_{LiMn}$[a] | 0.01 | −0.02 (±0.1) | −0.06 | −0.06 (±0.1) |

[a] The correlation coefficient, $c_{ij}$, between a pair of sites $i$ and $j$ is given by the statistical definition[30] of the correlation: $c_{ij} = (P_{ij} - \theta^2)/(\theta(1-\theta))$, where $P_{ij}$ is the probability that both sites $i$ and $j$ are occupied by the same atom type, and $\theta$ is its overall occupancy. Negative values of $c_{ij}$ indicate that the sites $i$ and $j$ tend to be occupied by different atom types.

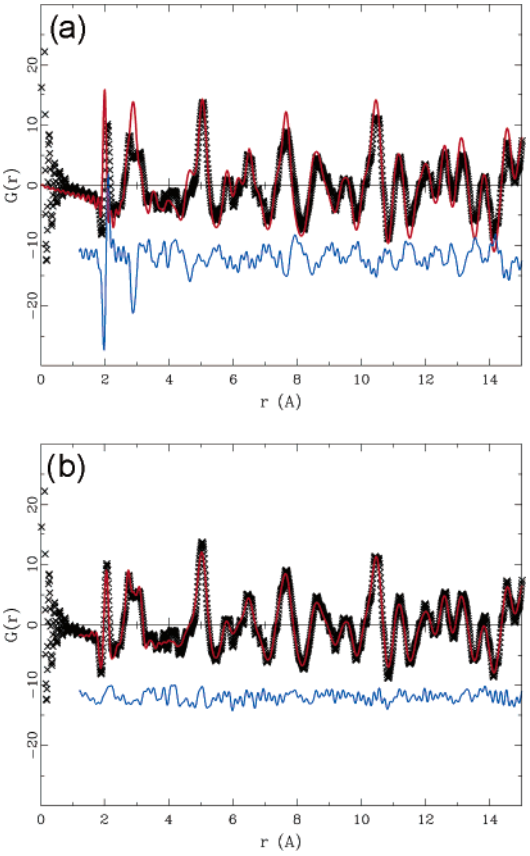


***Figure 7.*** Reverse Monte Carlo (RMC) results for $^7LiNi_{0.5}Mn_{0.5}O_2$ pristine material; (a) is the fit before the RMC calculations with the initial random cluster model, and (b) is after. The black crosses represent the experimental data, and the solid red line is the calculated PDF. The difference between the calculated and experimental patterns is shown in blue.

6). A $Ni^{2+}$−O bond length of 2.07 Å was obtained from the differential Ni PDF. This result is also consistent with EXAFS studies where an average $Ni^{2+}$−O bond length of 2.07 Å was found.[4] At least three peaks are seen at around 2.9 Å for the total PDF, which correspond to metal−metal, Li−metal, and O−O distances. All of these Pair Distribution Functions are poorly described by the PDF calculated using the ideal $LiCoO_2$ model, where a random distribution of Li, Ni, and Mn atoms in the TM layers is assumed (Figure 7a).

**Reverse Monte Carlo.** The Reverse Monte Carlo (RMC) technique was used in order to explore possible ordering of the Ni/Mn atoms and local distortions arising from different M−O bond lengths in the model used to fit the PDF data. The cell parameters ($a$ = 2.8947(6) Å and $c$ = 14.331(5) Å) were first refined by using the program PDFFIT[28] and the $LiCoO_2$ model. A cluster comprising 10 × 10 × 2 ($a \times a \times c$) unit cells (2400 atoms) was then built, which contained 10% of Li/Ni site exchange and the Li, Ni, and Mn atoms randomly distributed in the TM layers. RMC calculations were performed with the DISCUS program[29] by constraining the minimum bond lengths to 1.7 Å for Mn−O distances, 1.9 Å for Li−O and Ni−O distances, and 2.5 Å for all other distances. A peak sharpening parameter (determined by trial and error) was also used for values of $r$ smaller than 3.5 Å to account for correlated motion. Ni and Mn were swapped randomly in each step of the RMC, and all of the atoms were allowed to relax in the *ab* plane. If a generated move improved the fit, the move was accepted. Each atom swap and the relaxation procedure involved making a number of accepted moves corresponding to 10% of the total number of atoms in the cluster (i.e., 240 accepted moves for the 10 × 10 × 2 cluster). This procedure was repeated 100 times or until convergence was observed. At the end of the first set of RMC calculations, Li atoms were then randomly swapped with the Ni and Mn atoms, which did not result in a significant improvement to the fit. The final calculated PDF for the $^7Li(NiMn)_{0.5}O_2$ sample is shown in Figure 7b, and a clear improvement to the fit of the experimental data over that calculated from the random $LiCoO_2$ structure was obtained (Figure 7a). The nonzero values of the correlation coefficients show that the distribution of Ni, Mn, and Li cations in the TM layers is not random. The Ni/Mn correlation calculations (Table 3), $c_{NiMn}$, show a net tendency for Ni atoms to be surrounded by more Mn in the first coordination shell in the *ab* plane than in the random model since the correlation $c_{NiMn}$ becomes negative after the RMC calculations. The correlations involving the Li ions are not significant.

Three RMC calculations were performed on the $^7Li(NiMn)_{0.5}O_2$ sample using different initial random structures, and the results were very similar. RMC calculations performed with the data collected for the $^6Li(NiMn)_{0.5}O_2$ and $^7Li(^{ZERO}NiMn)_{0.5}O_2$ samples showed similar but less pronounced cation ordering (i.e., smaller values of the correlation coefficients). A second, larger (12 × 12 × 2 unit cell) cluster was then built to explore whether size of the cluster influences the

(28) Proffen, Th.; Billinge, S. J. L. *J. Appl. Crystallogr.* **1999**, *32*, 572.
(29) Proffen, Th.; Neder, R. B. *J. Appl. Crystallogr.* **1997**, *30*, 171.

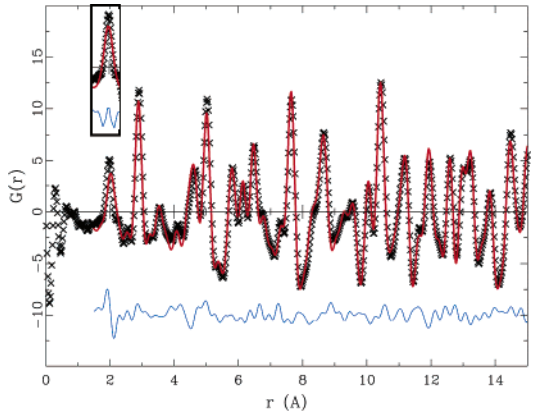


***Figure 8.*** Pair distribution function $G(r)$ of the $^7LiNi_{0.5}Mn_{0.5}O_2$ pristine material, obtained from X-ray diffraction (APS). The refinement was performed with PDFFIT software, using the random ($LiCoO_2$) structure. The black crosses represent the experimental data, and the solid red line is the calculated PDF. The difference between the calculated and experimental patterns is shown in blue below the data. The upper right inset shows the first peak of the PDF calculated from the structure obtained after the Reverse Monte Carlo (RMC) calculations.

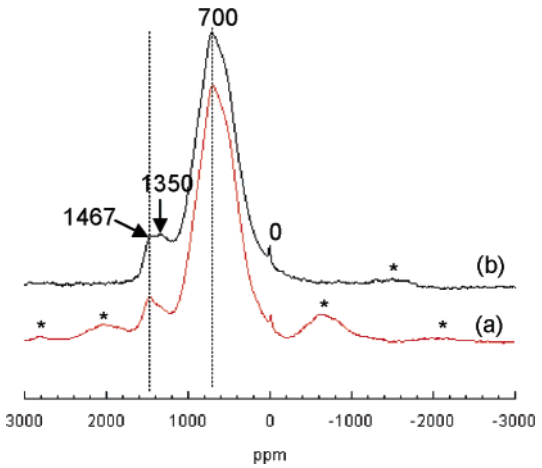


***Figure 9.*** $^6Li$ MAS NMR spectra of the $^6LiNi_{0.5}Mn_{0.5}O_2$ pristine material at spinning frequencies of (a) 39 and (b) 70 kHz. Dashed lines indicate the approximate shift positions of the $^6Li$ NMR resonances of $Li_2MnO_3$.[27] The sharp resonance at 0 ppm arises from diamagnetic impurities ($Li_2O$ for instance). The major isotropic resonances and spinning sidebands are marked with their shifts and asterisks, respectively.

cation orderings obtained from the RMC calculations (Table 3). A similar increase in the numbers of Ni−Mn pairs and decrease in Ni−Ni pairs over the numbers found in the random structure was observed. Only very small values of $c_{LiMn}$ and $c_{LiNi}$ were again observed, providing further confirmation that the Li correlations obtained in both clusters are not significant.

**Synchrotron XRD.** Figure 8 shows the PDF calculated with the synchrotron X-ray data collected at the APS for $^7Li(NiMn)_{0.5}O_2$ along with the refinement of the structure, performed using PDFFIT,[28] and the random $LiCoO_2$ structure (space group $R\bar{3}m$), with 10% Ni/Li site exchange. The calculated and the experimental patterns match reasonably well, except for the first peak, which corresponds to the Ni/Mn−O bond distances. The calculated X-ray PDF using the structure obtained from the RMC calculations, performed with the neutron diffraction data, fits this first peak better (inset in Figure 8), confirming that there are local distortions in the TM layers due to different M−O bond lengths that are not captured in the average $LiCoO_2$ structure model.

**NMR.** Figure 9 shows the $^6Li$ MAS NMR spectra of pristine $^6LiNi_{0.5}Mn_{0.5}O_2$, obtained with spinning frequencies of 39 and 70 kHz. The spectra are consistent with the work of Yoon et al.[8] and consist of two groups of resonances, one at around 700 ppm and the other between 1350 and 1467 ppm. As shown in our previous work,[31,32] the shifts are dominated by the hyperfine interaction (Fermi contact) between the lithium nuclear spins and the unpaired electrons located on the TM ions. On this basis and by comparison with the chemical shifts for $Li_2MnO_3$, the two groups of resonances were assigned to Li in Li layers and in TM layers, respectively. A value for the concentration of Li in TM layers of 9 ± 2% of the total Li content was determined by integration of the intensities of the different signals. The concentrations obtained from the spectra obtained at the two spinning speeds were similar, within experimental error, and consistent with the numbers determined by neutron diffraction.

The Li spectrum of $Li_2MnO_3$ contains a resonance at approximately 1450−1500 ppm, the exact value depending on the temperature of the sample, which has been assigned to the Li ions in the $[Li_{1/3}Mn_{2/3}]$ layers. On this basis, the resonance at 1467 ppm was assigned to Li local environments near six $Mn^{4+}$ ions in the first cation coordination shell ($LiMn_6$) and the resonance at 1350 ppm to environments containing five $Mn^{4+}$ ions, such as $LiMn_5Ni$.[9] Environments such as $LiMn_4Ni_2$, which give rise to resonances at lower frequencies (approximately 1000−1150 ppm), are clearly present in much lower concentrations. The good agreement between the concentrations of $Li^+$ ions in the TM layers as determined by NMR and diffraction indicates that we have accounted for the majority of Li ions in the TM layers and that the large resonance assigned to the Li ions in the lithium layers is not obscuring any weaker resonances due to different Li local environments in the TM layers. The assignment of the 1350 ppm resonance is not definitive, as simple predictions lead to an estimate of 1250−1200 ppm for the shift of this resonance, assuming that $Ni^{2+}$ ions in the first cation coordination shell give rise to no or weak negative shifts.[9] This is clearly lower than the experimentally observed shift. This may either be due to small differences in Li−O−M bond angles in the Li local coordination shell, residual magnetic interactions between the paramagnets, or the presence of $Ni^{2+}$ ions in the lithium layers, as discussed in some detail in our earlier papers.[9] Li ions in honeycomb versus flower structures may also be associated with slightly different shifts, suggesting that we cannot rule out the possibility that the 1350 ppm resonance arises from a slightly different $LiMn_6$ local environment from that giving rise to the resonance at 1500 ppm. Despite this, the NMR provides clear evidence that the majority of the Li ions in the TM layers occupy Li local environments containing five or more $Mn^{4+}$ ions.

**Electrochemistry.** Electrochemical experiments were performed to compare our sample with results presented in the literature. Figure 10 displays the voltage (V) versus capacity (mAh/g) curve for $^6LiNi_{0.5}Mn_{0.5}O_2$ cycled between 2.0 and 4.6 V using a C/20 rate in galvanostatic mode for eight cycles. The irreversible capacity for the first cycle is around 30 mAh/g, which is more than the capacity loss observed by Lu et al.[3] (15 mAh/g), giving a stable capacity of 130 mAh/g in cycles 2−8.

(30) Welberry T. R. *Rep. Prog. Phys.* **1985**, *48*, 1543.
(31) Lee, Y. J.; Grey, C. P. *J. Phys. Chem. B.* **2002**, *106*, 3576.
(32) Grey, C. P.; Dupré, N. *Chem. Rev.* **2004**, *104*, 4493.

***Table 4.*** Number of Li/Ni/Mn Pairs in the Transition Metal Layers (*ab* Plane) in the Two Different Ordering Schemes and Comparison with the 10 × 10 × 2 Cluster Calculations

| | First Coordination Shell | | | | Second Coordination Shell | | | |
|---|---|---|---|---|---|---|---|---|
| | Ordering Schemes | | 10 × 10 × 2 | | Ordering Schemes | | 10 × 10 × 2 | |
| | ordered flower | ordered honeycomb | before RMC | after RMC | ordered flower | ordered honeycomb | before RMC | after RMC |
| %Ni−Ni pairs | 16.67 | 13.75 | 16.4 | 12.0 | 16.67 | 20.50 | 16.9 | 21.1 |
| %Ni−Mn pairs | 50.00 | 47.50 | 42.0 | 50.5 | 33.33 | 25.00 | 41.1 | 33.5 |
| %Mn−Mn pairs | 16.67 | 18.75 | 23.2 | 19.1 | 33.33 | 37.50 | 23.7 | 27.2 |
| %Li−Mn pairs | 16.67 | 15.00 | 8.9 | 8.6 | 0 | 0 | 8.8 | 9.5 |
| %Li−Ni pairs | 0 | 5.00 | 8.61 | 8.94 | 16.67 | 14.00 | 8.44 | 7.72 |
| %Li−Li pairs | 0 | 0 | 0.89 | 0.89 | 0 | 3.00 | 1.06 | 1.06 |
| total | 100 | 100 | 100 | 100 | 100 | 100 | 100 | 100 |

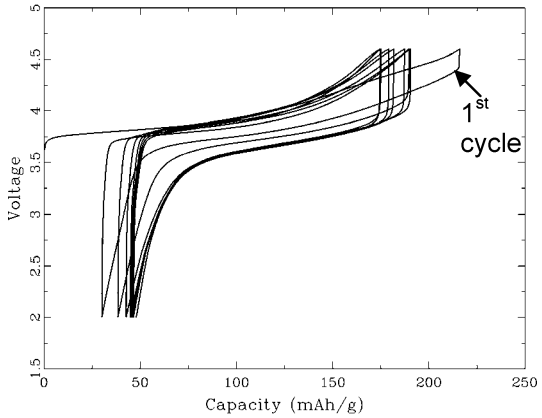


***Figure 10.*** Voltage versus specific capacity curve for $^6LiNi_{0.5}Mn_{0.5}O_2$ cycled (eight cycles) between 2.0 and 4.6 V using a C/20 rate, in galvanostatic mode.

This lower electrochemical performance may be due to differences in particle size coming from the synthesis method and in cell construction and cathode preparation techniques. However, the material shows electrochemical processes that are similar to those previously reported[3] with one major intercalation−deintercalation process at around 4.0 V, involving the $Ni^{2+}/Ni^{4+}$ redox couple. No additional redox processes were observed, indicating that the prepared sample is free of electrochemically active impurities.

## Discussion

The PDF approach makes use of all of the scattering data, including the superstructure peaks that cannot be indexed with the $LiCoO_2$ model used in the Rietveld structural refinement. This PDF data clearly reveal local distortions in the metal layers resulting in different M−O bond lengths. Use of different isotopes, in combination with the neutron scattering experiments, allows the different M−O bond lengths from the three different metals (Li, Mn, and Ni) to be distinguished. Again, the small local distortions are not captured in the average $LiCoO_2$ structure but are seen in the structural model that emerges from the RMC calculations. It is not feasible to refine the structure by using this model as the initial structural input, due to the large number of parameters that need to be refined in this low symmetry model.

Both the RMC and NMR results show a nonrandom distribution of cations in the TM layers. The Ni atoms are, on average, surrounded by 1.72 Ni, 3.64 Mn, and 0.64 Li ions and the Mn atoms by 3.11 Ni, 2.36 Mn, and 0.53 Li ions, based on the results shown in Table 3 for the 10 × 10 × 2 cluster. Similar results are obtained for the larger cluster. In the second cation coordination sphere, the correlation calculations suggest the opposite tendencies, the Ni atoms tending to avoid Mn atoms. On average, the Ni atoms are surrounded by 3.03 Ni, 2.41 Mn, and 0.56 Li ions and the Mn atoms by 2.07 Ni, 3.35 Mn, and 0.58 Li ions. In contrast to the NMR results, the correlations seen for the Li environment in the transition metal layers are less significant and are barely within the estimated standard deviations. Thus, no predictions concerning the Li local environments can be made from the RMC calculations. This lack of sensitivity is ascribed to the low concentrations of Li ions in the TM layers and the low scattering factors of this ion in contrast to those of Ni and Mn.

The PDF results can be compared with numbers calculated for the different ordering schemes proposed to date (honeycomb structure and flower structure; Figure 2) from first-principles calculations, NMR, and TEM studies.[8−10,27] This comparison is shown in Table 4. The composition of transition metal layers of the flower structure is ($LiNi_5Mn_6$), and thus these layers contain a lower Li concentration of only 8.3% Li (and a higher concentration of Ni of 41.7%). Comparing the numbers of Ni−Mn different pairs in both first and second cation coordination shells, the increase (first) and decrease (second) of the number of pairs from before to after the RMC calculations suggests nonrandom ordering that is similar to that found in either the flower or honeycomb layers. The changes in the numbers of Mn−Mn and Ni−Ni pairs following the RMC calculations are also in agreement with either of these ordering schemes. The higher concentration of Ni−Ni pairs in the flower structure arises, in part, from the higher concentration of Ni in the transition metal layers in this structure. Although the changes in M−M contacts from those of the random structure are consistent with the two models, the fit with either of the two models is not good enough to allow us to distinguish between the honeycomb and flower schemes. Furthermore, there is no evidence for ordering around the Li, which is in disagreement with these two models.

The NMR results may similarly be compared with the two models. Given that we observe two resonances that are assigned to the $Li(OMn)_6$ (1467 ppm) and $Li(OMn)_5(Ni)$ environments (1350 ppm), which occur with intensity ratios of approximately 1:1, and account for approximately 9% of the total Li content, we can calculate values for the numbers of Li−Mn and Li−Ni pairs of 16.5 and 1.5%, respectively. These values are very different from those for the random structure and are significantly closer to those calculated for the flower than for the honeycomb structure. In particular, the honeycomb structure

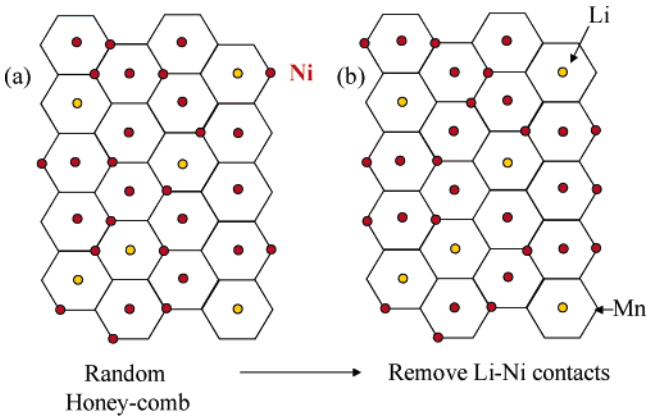


***Figure 11.*** (a) Honeycomb representation of the transition metal layers for $Li(NiMn)_{0.5}O_2$ with 10% of Li/Ni site exchange, where the atoms are distributed randomly. The yellow circles and the red circles represent Li atoms and Ni atoms, respectively. The Mn ions occupy empty corners of the hexagons (i.e., positions that do not contain circles). The Ni ions occupying the Mn sites of the honeycomb array have been moved in (b) so as to minimize the number of $Li(OMn)_4(ONi)_2$ local environments. The development of flowerlike arrangements (i.e., Li surrounded by a hexagon of Mn and a larger hexagon of Ni ions) is seen.

contains large concentrations of environments, such as $Li(OMn)_4(ONi)_2$ (>29% of the total Li environments; Figure 11), which are not observed experimentally by NMR. A similar observation was made in our analysis of the material, $Li[Ni_{1/3}Mn_{5/9}Li_{1/3}]O_2$, where again fewer of these environments were observed experimentally than predicted based on the honeycomb model.[9] Here, we explained these results by suggesting that the strong tendency for $Li^+-Ni^{2+}$ avoidance resulted in regions rich in Ni and Mn and regions comprising the $Li(OMn)_6$ and $Li(OMn)_5(ONi)$ clusters. This suggestion is consistent with the flower model of ordering.

Thus, our two experimental probes of local structure provide constraints on the ordering schemes seen in these materials. The lack of Li ordering seen by PDF indicates that this method has not captured all the details of the structure. However, the much larger neutron scattering factors of the Ni atoms suggests that the ordering around this element is essentially correct. Taken together, the results indicate ordering schemes similar to those expected for honeycomb and flower arrangements. Starting from the honeycomb structure, which generates concentrations of M−M′ pairs (M, M′ = Ni, Mn) that are close to those obtained by PDF, and imposing the constraints obtained by NMR (few or no $Li(OMn)_4(ONi)_2$ environments) (while maintaining the PDF constraints for the Ni and Mn contacts), we generate structures that resemble disordered flower structures. This is illustrated in Figure 11. Thus, the joint use of NMR and PDF methods provides strong evidence for nonrandom ordering of the ions in the transition metal layers. More work is still needed to model even larger structures and to use constraints from NMR directly in our RMC studies to develop even more detailed and accurate models of structure. These studies are in progress.

## Conclusions

NMR and Pair Distribution Function (PDF) analysis represent two complementary techniques, which allow the local environments and the short-range ordering in positive electrode (battery) materials to be investigated. The PDF method, like EXAFS, can be used to determine bond distances, providing insights into the oxidation states of cations and local distortions that are not captured in the average models of structure obtained by diffraction. Furthermore, the PDF technique is not limited to the first coordination shell and can give additional information about the local ordering in more distant coordination shells and provide structural parameters. Unlike EXAFS, where it is not possible to distinguish between M−Ni and M−Mn contacts, these contacts can be resolved in the PDF data taken from neutron experiments, due to the very different scattering factors of these elements. Use of different isotopes, with different scattering factors, allows definitive assignments of different M−O bond lengths to be made. Ordering of Ni, Mn, and Li atoms in the transition metal layers was detected in $Li(NiMn)_{0.5}O_2$; Ni atoms tend to be surrounded by more Mn atoms in the first coordination shell and by Li and Ni atoms in the second coordination shell, while Mn atoms are surrounded by Li and Ni atoms in the first coordination shell and by Mn atoms in the second coordination shell. These results were combined with data obtained from NMR to develop a detailed model of the structure. The application of this joint NMR−PDF analysis approach to many battery systems may be readily envisaged.

**Acknowledgment.** The work was supported by the Assistant Secretary for Energy Efficiency and Renewable Energy, Office of FreedomCAR and Vehicle Technologies of the U.S. Department of Energy under Contract No. DE-AC03-76SF00098, via subcontract No. 6517749 with the Lawrence Berkeley National Laboratory. This research was partially supported by COMPRES, the Consortium for Materials Properties Research in Earth Sciences under NSF Cooperative Agreement EAR 01-35554. The ISIS Facility of the Rutherford Appleton Laboratory is thanked for access to GEM. Use of the Advanced Photon Source was supported by the U.S. Department of Energy, Office of Science, Office of Basics Energy Sciences, under contract No. W-31-109-Eng-38. We thank Wonsub Yoon, Meng Jiang, Michael Lufaso, and Gerbrand Ceder for helpful discussions, and Laurent Chapon and Matthias Gutmann for their help in neutron data analysis. Ivo Heinmaa is thanked for running the very fast MAS spectrum.

JA050697U